Hindawi
Advances in Civil Engineering
Volume 2021, Article ID 6612886, 16 pages
https://doi.org/10.1155/2021/6612886

Research Article

Cyclic Behavior and Modeling of Bolted Glulam Joint with Cracks Loaded Parallel to Grain

Jing Zhang,[1] **Zhi-Fang Liu**,[2] **Yong Xu**,[1] **Mai-Li Zhang**,[1] **and Liu-Cheng Mo**[1]

[1]*Department of Structural Engineering, Guangzhou University, Guangzhou 510006, China*
[2]*Guangdong Architectural Design & Research Institute Co., Ltd., Guangzhou 510006, China*

Correspondence should be addressed to Jing Zhang; zhangjinggz@163.com

Received 19 November 2020; Revised 2 December 2020; Accepted 2 March 2021; Published 13 March 2021

Academic Editor: Arnaud Perrot

Copyright © 2021 Jing Zhang et al. This is an open access article distributed under the Creative Commons Attribution License, which permits unrestricted use, distribution, and reproduction in any medium, provided the original work is properly cited.

Under varying humidity and temperature conditions, with the constraint of metal fasteners to wood shrinkage, cracks along the bolt lines are generally observed in bolted glulam joints. A three-dimensional (3D) numerical model was established in software package ANSYS to investigate the cyclic behavior of bolted glulam joints with local cracks. A reversed cyclic loading was applied in the parallel-to-grain direction. The accuracy of numerical simulation was proved by comparison with full-scale experimental results. Typical failure modes were reproduced in the numerical analysis with the application of wood foundation zone material model and cohesive zone material model. The effect of crack number and length on the hysteretic behavior of bolted glulam joints was quantified by a parametric study. It was found that initial cracks impair the peak capacity and elastic stiffness of bolted glulam joints significantly. More decrease in capacity was observed in joints with more cracks, and longer cracks affect elastic stiffness more dramatically. Moreover, with the existence of initial cracks, the energy dissipated and equivalent viscous damping ratio of bolted joints are reduced by 24% and 13.3%, respectively.

1. Introduction

Connections are always recognized as the weakest part of timber structures. It was reported that nearly 80% of structural collapses arise from connections [1]. The mechanical behavior of joints significantly affects resistance, durability, and energy dissipation of timber structures. Dowel-type joints, an effective fastening technique extensively applied in actual engineering, have attracted tremendous research interest. Extensive experimental and numerical studies on the static [2–5] and cyclic behavior [6–8] of dowel-type joints have been conducted and available in the literature. The load-carrying capacity and failure modes of bolted joints are related to material behavior, geometry, and loading type. Relatively large energy dissipation and ductile behavior could be achieved with small diameter bolts, and slender bolts are preferred in the bolted glulam joints in order to avoid brittle failure modes [9].

In terms of modeling the mechanical behavior of bolted glulam joints, several methods have been proposed by previous researchers. An analytical method named Beam-on-Foundation model was first applied [10] and modified [11] to predict the monotonic strength and hysteretic behavior of nailed and bolted wood connections. To represent the dynamic response of timber connections, hysteresis models such as Bouc-Wen-Baber-Noori model [12], Florence model [13], and Pinching4 [14] were employed in structural analysis. A three-dimensional (3D) finite-element-based model is a recent and efficient approach to estimate the behavior of bolted glulam joint. Complete strain and stress distributions can be obtained and observed from numerical analysis. In the numerical modeling, a reasonable definition of material behavior is particularly important to achieve relatively accurate numerical results. To take into account the localized crushing behavior of wood underneath the fasteners, a foundation zone around the fasteners with weakened material properties was defined in a two-dimensional numerical model [15], and it was extended to 3D FE models by Hong [16]. To consider the progressive failure of wood in bolted glulam joints, several failure criteria were proposed by previous researchers. In the

3D numerical model of a single-bolt connection developed by Moses and Prion [17], anisotropic plasticity material model was defined for wood in compression and Weibull Weakest Link Theory was applied to consider brittle failure. It was indicated that the force-displacement relationship was predicted well, while the ultimate loads were underestimated. Hill yield criterion and maximum stress failure criterion were selected by Kharouf [18] when establishing a numerical model of timber joints, and it was found that failure modes and deformation predicted by numerical analysis fit well with experimental results. Hoffman failure criterion was applied by Xu et al. [19] to take into account the damage evolution of wood. Tsai-Wu failure criterion is able to consider the difference between tension and compression strengths of wood [20], while stress interaction coefficients defined in the criterion are difficult to determine [21]. The application of cohesive zone material model into bolted glulam joints has been attempted by several researchers [22–24]. With the definition of mixed mode damage onset and propagation criteria, it was proved to be a powerful tool to simulate splitting and row shear commonly observed in bolted joints.

Extensive researches have been conducted on mechanical behavior and strength enhancement of bolted glulam joints as above. However, little attention was paid to the mechanical behavior of bolted glulam joints with local cracks. Shrinkage cracks are generally observed in bolted glulam joints due to their sensitivity to varying relative humidity of the environment. Shrinkage and swelling strains of wood are restrained with the existence of steel fasteners in the joint area, and cracking of wood is easily caused by perpendicular-to-grain restrained stress [25]. Previous researches have proved that the capacity, stiffness, and ductility of bolted glulam joints are decreased by initial cracks under monotonic loading, and failure modes of bolted glulam joints switched from ductile failure with bolt yielding to brittle failure of wood [26, 27]. It is essential to further investigate the influence of initial cracks on the cyclic behavior of bolted glulam joints. In respect of numerical modeling, the complexity of contact problems and material behavior provides challenges of convergence. Even though some 3D numerical analysis has been conducted on the monotonic behavior of bolted glulam joints, few attempts have been conducted to model the cyclic behavior of timber joints by 3D numerical analysis.

To reveal the influence law of cracks on the cyclic behavior of bolted glulam joints intuitively, a 3D numerical model was established in this paper. Hill yield criterion and wood foundation model were applied to simulate the behavior of wood in compression and wood around fasteners, respectively. Brittle failure of wood and propagation of initial cracks were modeled with the application of cohesive zone material model. Several contact pairs were defined to model the interaction between different parts in the joint, and reversed cyclic loading was applied in the parallel-to-grain direction. The experimentally observed failure modes and hysteretic curves were used to verify the numerical results, and the influence of different crack patterns was explored by a parametric study.

2. Development of Finite-Element-Based Model

2.1. Material Modeling. To model the mechanical behavior of wood in compression, the transversely isotropic plastic material model was defined with the application of the Hill yield criterion, which had been incorporated in business software ANSYS. To take into account the embedment behavior of wood underneath bolts, a foundation zone was set around bolts with a radius of 1.8-time bolt diameter. The generalized Hill plasticity model with anisotropic hardening rule was applied to represent the mechanical behavior of wood foundation. 1% of initial modulus was taken as tangent modulus of hardening segment. With embedment tests loaded in perpendicular- and parallel-to-grain directions, a bilinear relationship between load per unit length and deformation was obtained, as shown in Figure 1, and nominal yield stress and strain of foundation zone were calculated by

$$\varepsilon_{\text{nom.}} = \frac{W_y}{d},$$
$$\sigma_{\text{nom.}} = \frac{P_y}{d}, \tag{1}$$
$$K = \frac{P_y}{W_y},$$

where $\varepsilon_{\text{nom.}}$ and $\sigma_{\text{nom.}}$ are the nominal yield strain and stress (MPa) of wood foundation, respectively; W_y and P_y are the deformation (mm) and yield load (N/mm) in Figure 1. Further calibration was conducted to derive effective foundation parameters. Shear modulus and yield strain were calculated according to a theoretical formula given in [28], as presented in

$$G_{ij} = G_{ji} = \frac{\sqrt{E_i \cdot E_j}}{2 \cdot \left(1 + \sqrt{\nu_{ij} \cdot \nu_{ji}}\right)},$$
$$\left(\gamma_y\right)_{ij} = \left(\gamma_y\right)_{ji} = \frac{\left(\sigma_{\text{int.}}\right)_i}{1.98 \cdot E_i} \cdot \sqrt{\frac{E_i}{G_{ij}}}, \tag{2}$$

where G is the initial shear modulus; E is the effective modulus of wood foundation; ν is Poisson's ratio; γ_y is the shear yield strain; and $\sigma_{\text{int.}}$ is the intercept of the second linear portion in the bilinear stress-strain relationship. For bolts and steel plate existing in bolted glulam joints, elastic modulus and Poisson's ratio were taken as 210,000 MPa and 0.3, respectively. The isotropic plastic material model with a bilinear constitutive relationship was defined, as shown in Figure 2.

To simulate the propagation of initial cracks and brittle failure (i.e., splitting and row shear) of wood in bolted glulam joints, surface-to-surface contact pairs with elements CONTA174 and TARGE170 were defined on the predicted cracking path. To characterize the constitutive relationship of the interface, the cohesive zone material model with damage initiation and growth criteria was implemented in the numerical model. As shown in Figure 3, a bilinear traction separation law was defined, and mode I and II

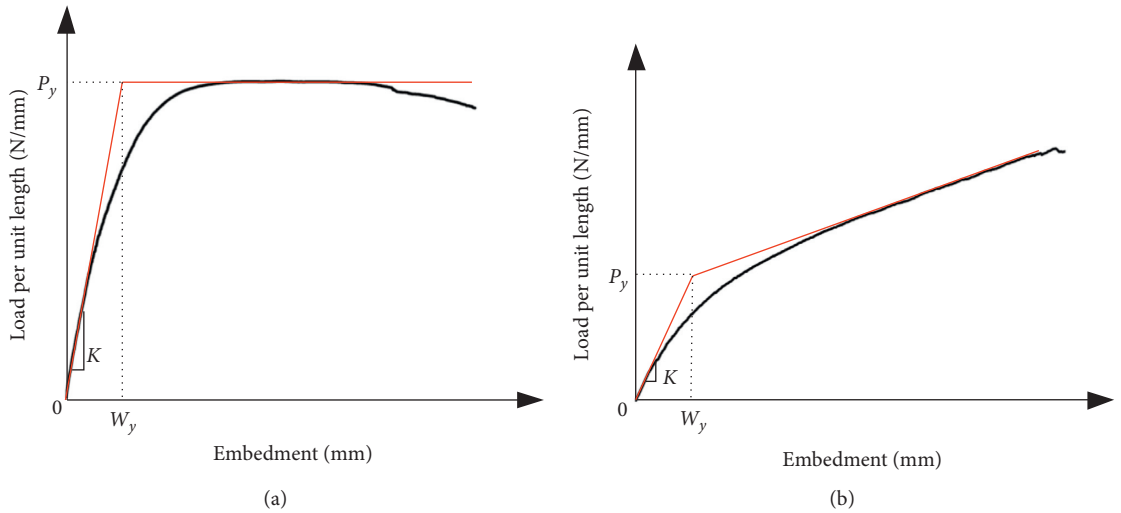

Figure 1: Load-embedment curves obtained from embedment tests and corresponding bilinear relationships. (a) Parallel to grain. (b) Perpendicular to grain.

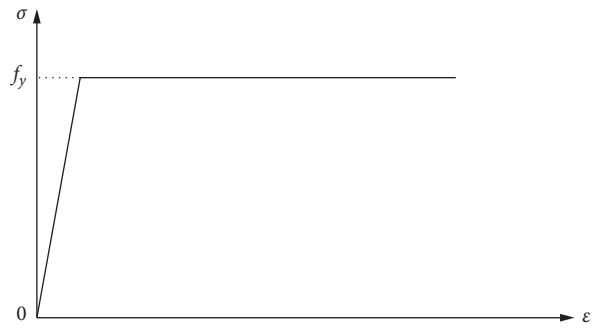

Figure 2: Bilinear stress-strain relationship for steel material.

fractures caused by perpendicular-to-grain tensile stress and longitudinal shear stress were taken into account. In Figure 3, K_n and K_t represent normal and tangential contact stiffness, respectively. A linear softening segment was observed after peak point corresponding to material strengths $f_{t,90}$ and f_s, and complete debonding occurs when reaching critical values of relative displacement u_n^c or u_t^c. Mixed mode fracture was considered in the analysis with a combined energy criterion, expressed as follows:

$$\frac{G_{\mathrm{I}}}{G_c^{\mathrm{I}}} + \frac{G_{\mathrm{II}}}{G_c^{\mathrm{II}}} = 1, \tag{3}$$

where G_{I} and G_{II} indicate fracture energies in modes I and II and G_c^{I} and G_c^{II} represent respective critical values, which are obtained from Double Cantilever Beam (DCB) test and End Notched Flexure (ENF) test, respectively, with the application of compliance combination method. In this numerical model, a small fictitious viscosity is introduced to avoid convergence difficulties.

2.2. Finite-Element Model. A 3D finite-element model of bolted glulam joints was established in FE-software ANSYS. Eight-node solid element SOLID185 was applied to embody the joints. To model the interaction between bolts and steel plate, timber and bolts, timber and steel plate, and timber and steel gasket, surface-to-surface contact pairs were defined with CONTA174 and TARGE170 elements. For bolt-to-steel plate and wood-to-steel contacts, coefficients of friction were taken as 0.001 and 0.3, respectively [29]. An example of the distribution zone of different material models was presented in Figure 4. The transversely isotropic plastic material model with the Hill yield criterion was induced to represent the compressive behavior of wood in the joint. Wood foundation zone material model was applied to simulate the embedment behavior of wooden parts surrounding the bolts, and the radius of the cylinder was set to be 1.8 d, where d indicates the bolt diameter. The mechanical behavior of bolts and steel plate was modeled with a bilinear isotropic plastic constitutive relationship. To simulate the splitting and plug shear failure of wood in the joint area, crack growth paths along the bolt lines were predicted based on experimental observations [23], as shown in Figure 5. The width of wooden parts plugged out by bolt load was assumed to be $dsin\phi$, and $\phi = 30^\circ$ was determined based on the friction between bolt and wood as given in [30]. For bolted glulam joints with initial cracks, hard contact conditions were defined to simulate the opening and closure of initial cracks. All the material constants applied in the analysis were listed in Table 1.

To study the cyclic behavior of bolted glulam joints, a gap of 30 mm was set between the top surface of steel plates and the slot, as presented in the side view of Figure 4. The bottom surface of the slotted-in steel plate was fixed, and a reversed cyclic loading was applied on the top end of glulam specimens. The loading protocol recommended in EN 12512 standard [31] was applied, as presented in Figure 6. The parameter V_y required for cyclic loading protocol was determined as yield displacement under monotonic loading. The amplitudes of loading cycles ranged from $0.25V_y$ to $6.0V_y$, the single cycle was considered for the amplitudes $0.25V_y$ and $6.0V_y$, and three cycles were repeated for other amplitude levels.

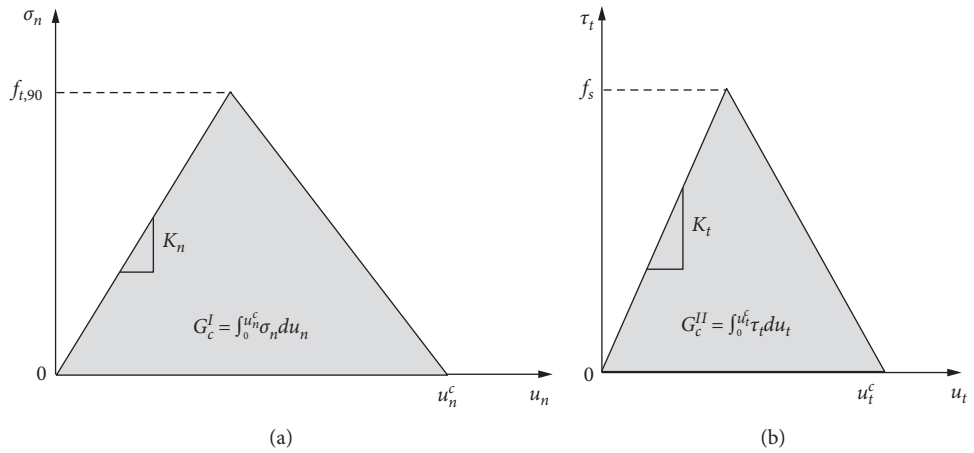

Figure 3: Cohesive zone material behavior. (a) Fracture mode I. (b) Fracture mode II.

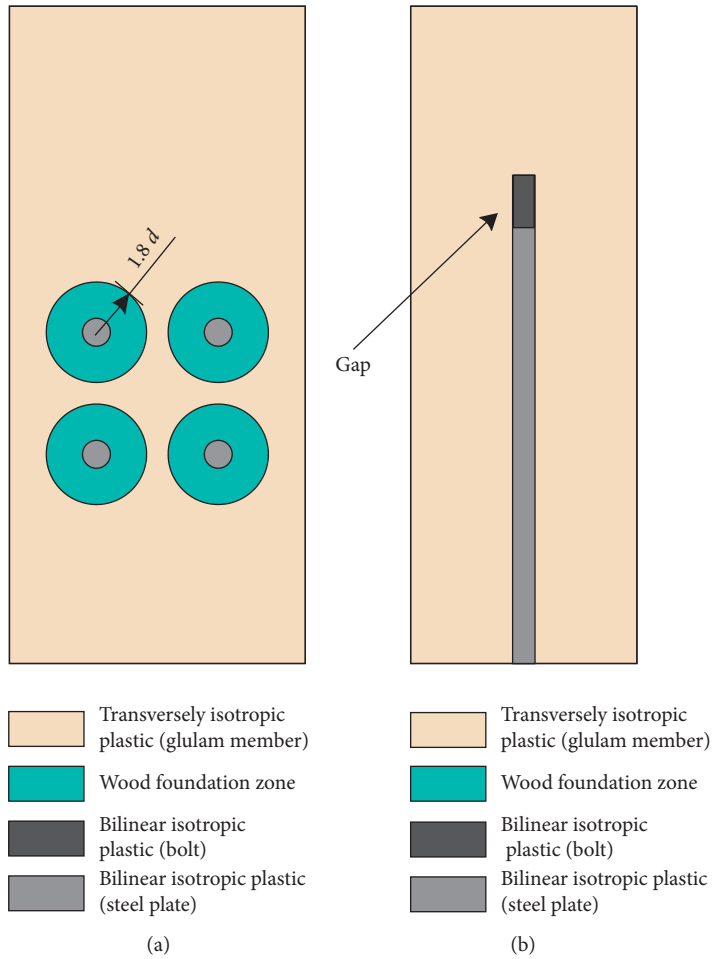

Figure 4: An example of the distribution zones of different material models. (a) Front view. (b) Side view.

3. Model Verification

To validate the feasibility of the numerical model, a bolted glulam joint with five replicates was manufactured and tested. The configuration of tested joints is presented in Figure 7. The width and thickness of glulam members are 200 mm and 100 mm, respectively. The slotted-in steel plates are 8 mm in thickness with a nominal yield stress of 235 MPa. Two bolts with a strength grade of 8.8 and a diameter of 12 mm are included in the joint, which has a nominal yield strength of

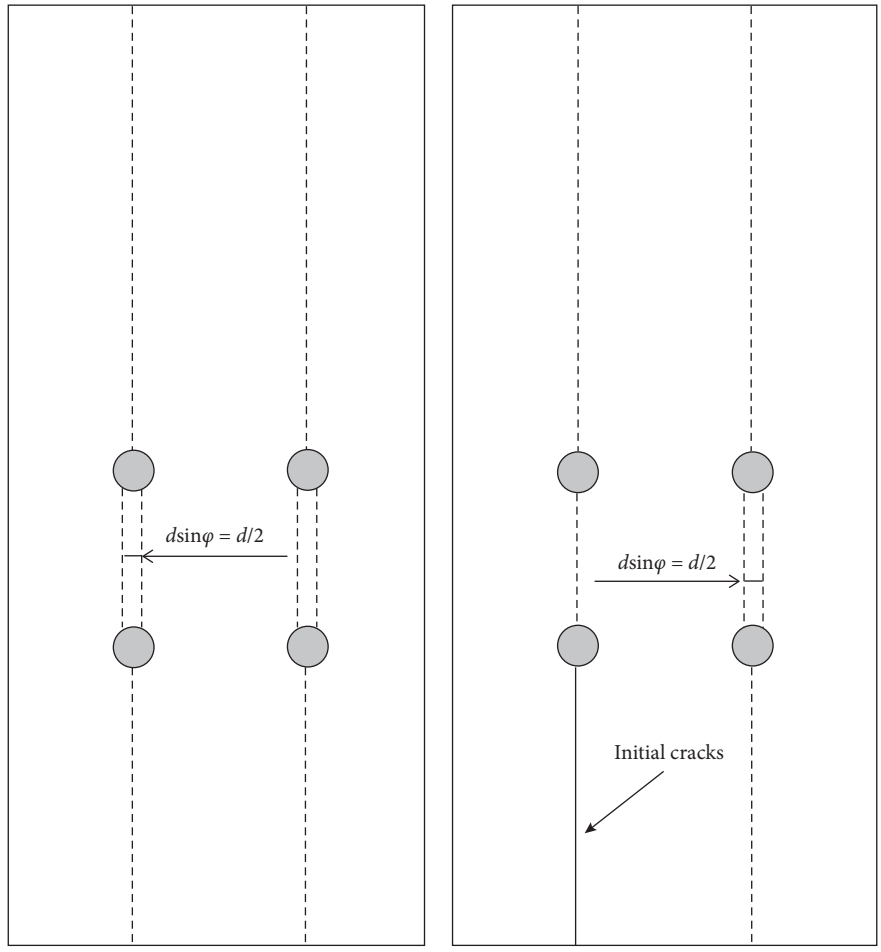

Figure 5: Fictitious fracture layers set in joints with four bolts. (a) Without initial cracks. (b) With initial cracks.

Table 1: Material constants applied in this model.

Component	Bolt	Steel plate	Wood	Wood foundation
Modulus of elasticity (N/mm^2)	$E = 2.1e5$	$E = 2.1e5$	$E_L = 1.02e4$ $E_{R;T} = 510$	$E_L = 1.04e3$ $E_{R;T} = 103$
Modulus of rigidity (N/mm^2)	—	—	$G_{LT;LR} = 845$ $G_{RT} = 80$	$G_{LT;LR} = 273$ $G_{RT} = 76$
Poisson ratio	$\nu = 0.3$	$\nu = 0.3$	$\nu_{LT;LR} = 0.37$ $\nu_{RT} = 0.44$	$\nu_{LT;LR} = 0.37$ $\nu_{RT} = 0.44$
Yield stress (N/mm^2)	$f_y = 640$	$f_y = 235$	$\sigma_L = 23.50$ $\sigma_{R;T} = 3.68$	$\sigma_L = 20.58$ $\sigma_{R;T} = 5.09$
Strengths (N/mm^2)	—	—	$f_{t;90} = 2.7$ $f_s = 5.7$	$f_{t;90} = 2.7$ $f_s = 5.7$
Fracture energies (N/mm)	—	—	$G_c^{\mathrm{I}} = 0.24$ $G_c^{\mathrm{II}} = 0.55$	$G_c^{\mathrm{I}} = 0.24$ $G_c^{\mathrm{II}} = 0.55$

640 MPa according to Chinese code [32]. As can be seen from Figure 8, under the cyclic loading, obvious bending deformation of bolts was observed in the bolted glulam joints.

The numerical model of the tested joint was established and the results obtained from numerical analysis were compared to experimental findings for verification purposes. The failure modes of bolted joints predicted by numerical

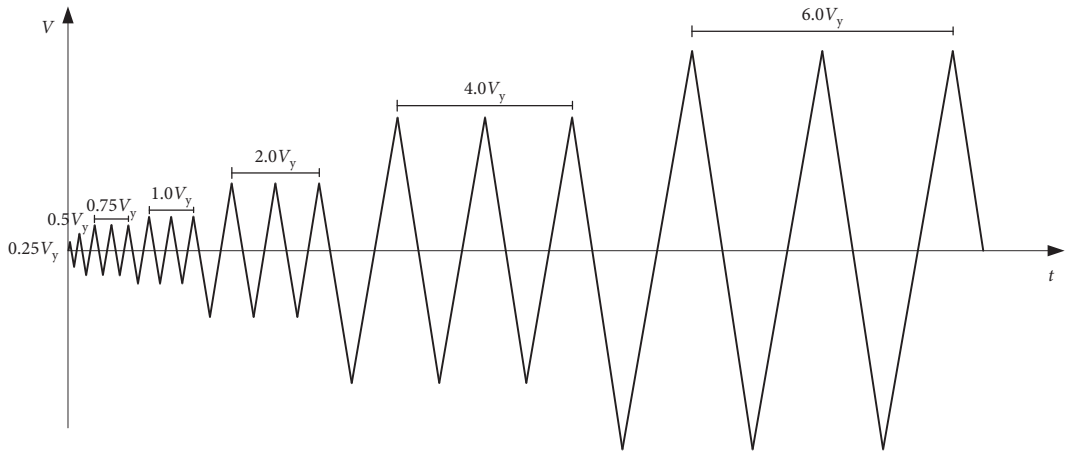

Figure 6: Loading protocol recommended in EN 12512 (2001).

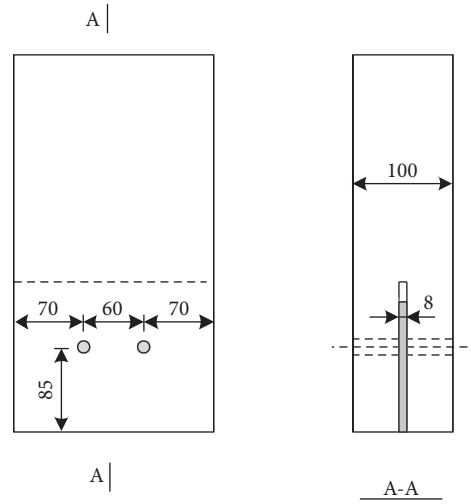

Figure 7: Detailed configurations of test bolted joint.

analysis are shown in Figure 8. Bolt bending deformation and embedment deformation of wood observed in the joint are quite similar to the experimental phenomenon. The comparison between the test obtained and the numerical predicted hysteretic curves was conducted and presented in Figure 9. As can be seen from the figure, the shape of the force-displacement hysteretic loops predicted by numerical analysis fit well with the test results. The deviation in displacement levels is caused by the difference between experimental obtained and numerical predicted yield displacement V_y under monotonic loading, which was related to the variability in wood properties and bolt clearance existing in test specimens. The mechanical parameters such as elastic stiffness and peak loading capacity are calculated and listed in Table 2. It can be seen that elastic stiffness obtained from the test is lower than the numerical results due to wood properties variation in the tested specimens. The experimentally obtained peak load-bearing capacity is slightly larger than the numerically predicted values, which is believed to relate to the discrepancy between the nominal and actual yield strength of bolts. The enclosed area of hysteretic loops was calculated to obtain the accumulative energy dissipation of the joints under reversed cyclic loading. As listed in Table 2, the numerical predicted energy dissipation is 1766.4 J, which is only 7% larger than the test value. It validates the reasonability of applying the numerical model to simulate the cyclic behavior of bolted glulam joints.

4. Parametric Study

To investigate the effects of crack patterns on the cyclic behavior of bolted glulam joints, a parametric study was conducted with the consideration of different bolt configurations. A single-bolt line with two bolts was included in Joint 1, as shown in Figure 10(a). The cross-sectional size of the glulam member is 120 x 90 mm, and the bolts are 12 mm in diameter with a nominal yield strength of 480 MPa. The geometric size of the glulam member in Joint 2 is identical to the tested joint, and the bolts are 16 mm in diameter with a nominal yield strength of 640 MPa, as presented in Figure 10(b). Different crack numbers and locations were considered in the analysis. The detailed information of crack patterns is shown in Figure 11. For crack patterns SB and ST in Joint 1, different crack lengths are considered and initial crack is cut through the bottom and top bolt, respectively. Initial cracks set on both sides of the steel plate are included in Joint 1 with crack patterns DB and DT. For crack patterns LS and LD in Joint 2, initial cracks along the left bolt line are set on single and both sides of the slotted-in steel plate, respectively. Initial cracks along both right and left bolt lines are included in the joints with crack patterns RLS and RLD.

4.1. Failure Modes and Hysteretic Curves. For initially perfect Joint 1, splitting failure of wood is observed under positive loading (i.e., tension load), as shown in Figure 12(a). Bolt yielding occurred under negative loading, as can be seen from the von Mises stress distribution of the middle cross section in Figure 12(b). In terms of the hysteretic curve, an obvious pinch phenomenon is observed from Figure 13(a), which is caused by the brittle failure of wood and plastic deformation of bolts. Under positive loading, a sudden drop of load-carrying capacity occurred at a loading amplitude level of 2.0 mm due to the splitting failure of wood.

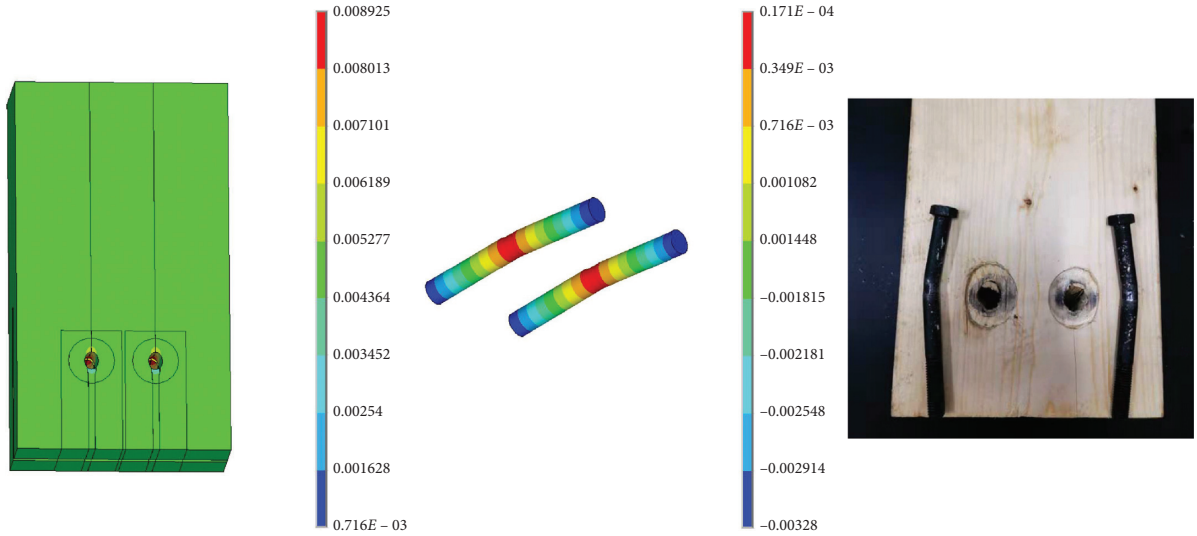

Figure 8: Failure modes of bolted glulam joint obtained from numerical analysis and experiment.

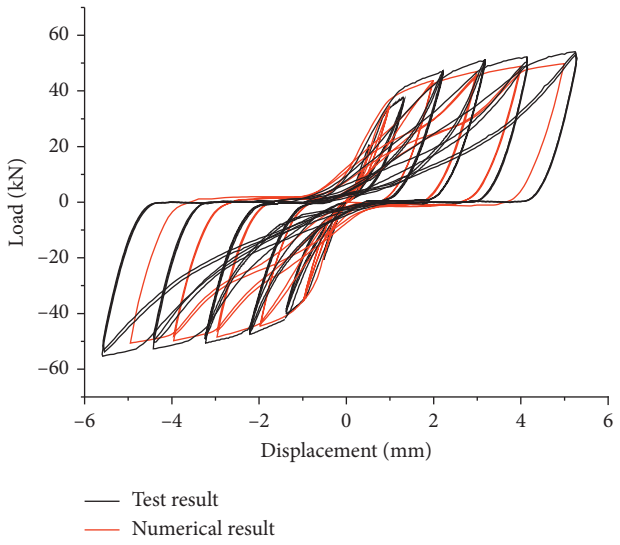

Figure 9: Comparison between experimentally obtained and numerical predicted hysteretic curves.

Compared to the mechanical behavior of the joint under positive loading, a more ductile performance is observed under negative loading. The joint with crack pattern DT exhibited a more pitched hysteretic behavior when compared with the initially perfect joint, as shown in Figure 13(b). The peak loading capacity and elastic stiffness are reduced by initial cracks. Under positive loading, a small decrease in capacity occurred when the displacement reaches 2 mm, which is caused by the propagation of initial cracks.

To investigate the effect of different numbers of cracks on the hysteretic behavior of bolted glulam joints, a comparison is conducted between Joint 1 with crack patterns SB and DB as presented in Figure 13(c). As can be seen from the figure, for Joint 1-SB with a single crack on one side of the steel plate, the brittle failure of wooden parts on the other side leads to the decrease of the load-carrying capacity from 30.7 kN to 19.2 kN. Compared to Joint 1-SB, a relatively lower peak capacity on the positive side is observed in Joint 1-DB with two initial cracks. Different crack lengths are considered in Figure 13(d), and the hysteretic curve of Joint 1-DB is compared to that of 1-DT. As can be seen from the figure, crack lengths only affect the elastic stiffness of bolted joints under positive loading. The initial crack in Joint 1-DB propagates from bottom bolt to top bolt at the displacement of 1 mm, and a slight decrease of capacity is observed in the figure. After this crack propagation, the same cracking conditions are obtained in these two joints, and thus the hysteretic curve of Joint 1-DB coincides with Joint 1-DT under further application of displacement load.

The main failure modes of initially perfect Joint 2 include the embedment failure of wooden parts around bolt holes and brittle failure of wood in the joint area, as shown in Figure 14. Obvious embedment deformation is observed before the occurrence of splitting failure of wood, as presented in Figure 14(a), while the bolts remain stiff and straight, and no significant bolt bending deformation is observed. The von Mises stress distribution of the middle section is given in Figure 14(c). It is indicated that only a slight portion of the bolts reaches the yield strength and the rest performs an elastic behavior.

Compared to Joint 1, a more significant pinch phenomenon is observed in the hysteretic curve of Joint 2, as shown in Figure 15(a), which is caused by the unrecoverable embedment deformation and splitting failure of wood. When the relative displacement of the initially perfect joint reaches 3.1 mm, splitting failure occurred along the bolt lines, and the capacity of the joint under positive loading decreases from 71 kN to 46 kN. In the loading cycle with an amplitude level of 6.0 mm, the peak capacity of the joint under positive loading is close to 60 kN. The capacity drops quickly in the unloading process, and the residual plastic deformation is around 4.3 mm. Nearly zero capacity is observed when the displacement declines from 4.3 mm to −2.5 mm under reversed loading due to the significant

Table 2: Mechanical parameters obtained from experimental and numerical results.

	Elastic stiffness (kN/mm)	Peak load (kN)	Accumulated energy dissipation (J)
Test result	38.0	52.9	1650.8
Numerical result	49.5	50.7	1766.4

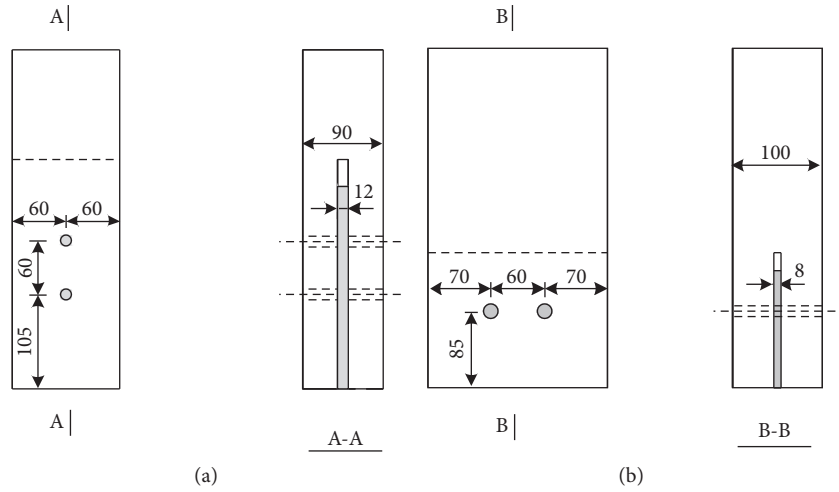

Figure 10: Two bolted glulam joints considered in the parametric study. (a) Joint 1. (b) Joint 2.

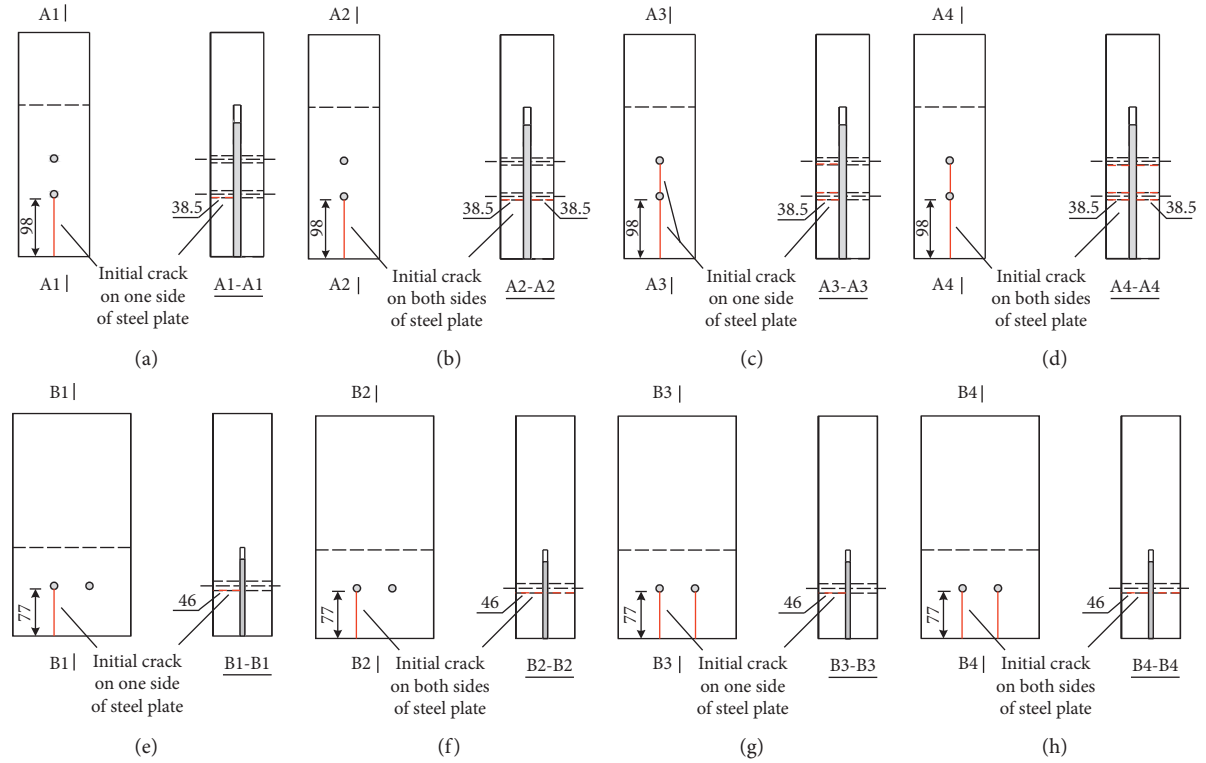

Figure 11: Different crack patterns considered in Joint 1 and Joint 2. (a) Joint 1-SB. (b) Joint 1-DB. (c) Joint 1-ST. (d) Joint 1-DT. (e) Joint 2-LS. (f) Joint 2-LD. (g) Joint 2-RLS. (h) Joint 2-RLD.

embedment deformation. By comparison with the initially perfect joint, the peak loading capacity and elastic stiffness of the joint with crack pattern RLD are impaired by initial cracks, as can be observed from the positive side of Figure 15(a). The propagation of cracks occurred at the displacement of 2.9 mm. In Figure 15(b), a comparison is

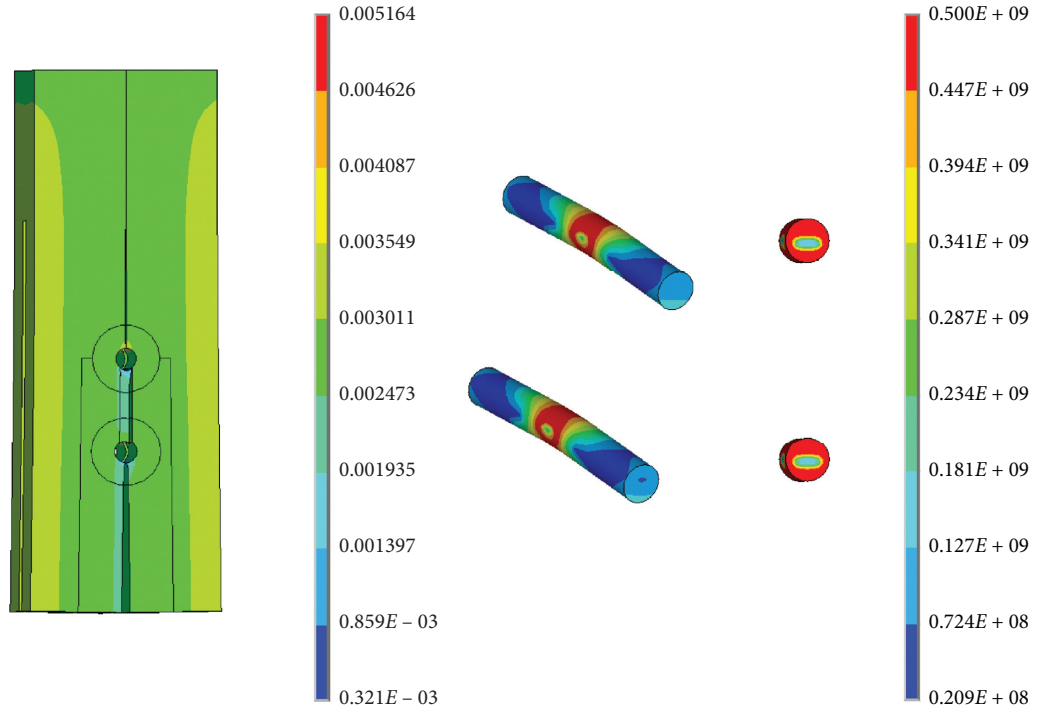

Figure 12: Failure mode of initially perfect Joint 1: (a) splitting failure of wooden parts; (b) von Mises stress distribution of bolts.

conducted between Joint 2 with crack patterns LD and RLD to explore the influence of different numbers of cracks. It can be seen that when compared with Joint 2-RLD including four cracks, a larger peak capacity is observed in Joint 2-LD with two cracks along the left bolt line. A drop of capacity in Joint 2-LD is observed at the displacement of 4.2 mm due to the splitting failure of wood along the right bolt line.

4.2. Skeleton Curves. The skeleton curves of Joint 1 are presented in Figure 16, which are obtained by connecting peak points of each primary loading cycle in the force-displacement hysteretic loops. Different numbers and lengths of initial cracks are considered in the comparison. As can be seen from Figure 16, the positive and negative sides of skeleton curves can be divided into three segments, respectively. A linear load-displacement relationship is observed in the first segment. Under positive loading, the stiffness of the linear segment is reduced by initial cracks when compared with the initially perfect joint, which is caused by the influence of crack opening on the interaction between bolts and wooden parts. The second segment is nonlinear, and stiffness attenuation is observed due to the occurrence of bolt yielding. After the peak point, a significant decrease in load-bearing capacity is observed from skeleton curves, which is caused by a brittle failure of wood in the joint area.

Mechanical parameters of Joint 1 under positive and negative loading were calculated and listed in Table 3, including elastic stiffness, yield force, yield displacement, peak capacity, ultimate displacement, and ductility ratio. The yield point was estimated based on ASTM D5764 [33], as shown in Figure 17. A straight line is drawn parallel to the linear segment and the offset is set as 5% of bolt diameter. The intersection point between the line and the skeleton curve is determined as the yield point. For envelope curves with the declining branch, the ultimate displacement is defined as the deformation corresponding to 80% of peak strength and the ductility ratio is calculated as ultimate displacement divided by yield displacement.

As can be seen from Figure 16 and Table 3, the peak loading capacity and initial stiffness of Joint 1 under positive loading are impaired by initial cracks, while negligible influence is observed on the mechanical performance under negative loading. Under positive loading, the peak capacity of Joint 1-SB and Joint 1-DB is 31.4 kN and 29.4 kN, respectively. Compared to the initially perfect joint, the decreasing ratio of capacity can be up to 21.8%, which is calculated by dividing the decrease by the corresponding value of the initially perfect joint. Further, it is indicated that more cracks lead to a more significant reduction in peak loading capacity. In terms of elastic stiffness, when compared to Joint 1-SB, lower stiffness is observed in Joint 1-DB with two initial cracks.

Different crack lengths are considered in Joint 1-DB and Joint 1-DT. As can be seen from Table 3, a similar peak capacity is found for these two joints, which indicated that crack lengths have little influence on the peak capacity of bolted joints. The elastic stiffness of Joint 1-DB and Joint 1-DT is 24.5 kN/mm and 17.2 kN/mm, respectively. Under positive loading, a longer crack reduces the elastic stiffness of bolted joint more significantly. When compared with an

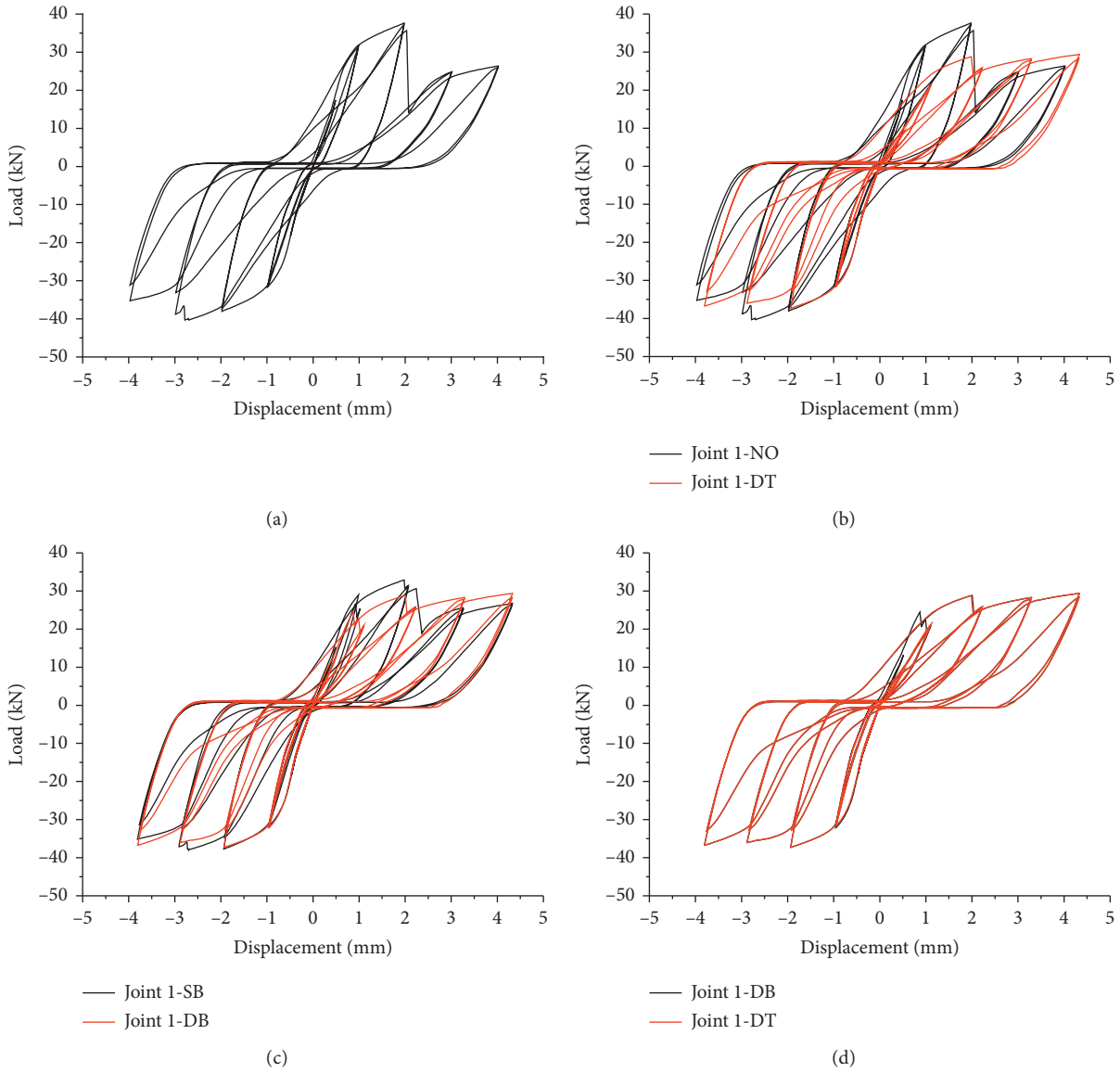

Figure 13: Hysteretic curves of Joint 1: (a) initially perfect Joint 1; (b) comparison between initially perfect Joint 1 and Joint 1-DT; (c) comparison between Joint 1-SB and Joint 1-DB; (d) comparison between Joint 1-DB and Joint 1-DT.

initially perfect joint, the decreasing ratio of elastic stiffness can be up to 47.4% with the existence of two cracks through the top bolt. In terms of ductility ratio, it can be found from Table 3 that the ductility ratio of the initially perfect joint is lower than the joints with initial cracks. Brittle failure of wood under external load leads to a sudden drop of capacity in the initially perfect joint, while a smoothing skeleton curve is realized in Joint 1-DB and Joint 1-DT with the occurrence of crack propagation instead of brittle failure of wood. The ductility ratio of Joint 1-DB and Joint 1-DT is 2.85 and 2.32, respectively.

The skeleton curves and mechanical parameters of Joint 2 are presented in Figure 18 and Table 4, respectively. Similar to Joint 1, the reduction in the peak loading capacity and elastic stiffness is observed with the existence of initial cracks. As can be seen from the table, the peak capacity of Joint 1-LS and Joint 1-RLD under positive loading is 68.4 kN and 60.1 kN, respectively. Compared to an initially perfect joint with a capacity of 71.4 kN, the decreasing ratio of capacity can be up to 15.8%. With initial cracks on both bolt lines, the elastic stiffness of bolted joints declines from 49.6 kN/mm to 40.2 kN/mm with a decreasing ratio of 19.0%. Compared to Joint 1, the influence of initial cracks is less significant on the peak capacity and elastic stiffness of Joint 2, while initial cracks impair the ductility behavior of Joint 2, contrary to the observed trend in Joint 1. Similar ultimate displacement is observed in the joints with or without initial cracks, as shown in Table 4.

4.3. Stiffness Degradation. Under reversed cyclic loading, the stiffness of bolted glulam joints declined gradually with increased loading amplitudes with wood crushing or bolting yielding. The secant stiffness of primary loading cycles was calculated as follows:

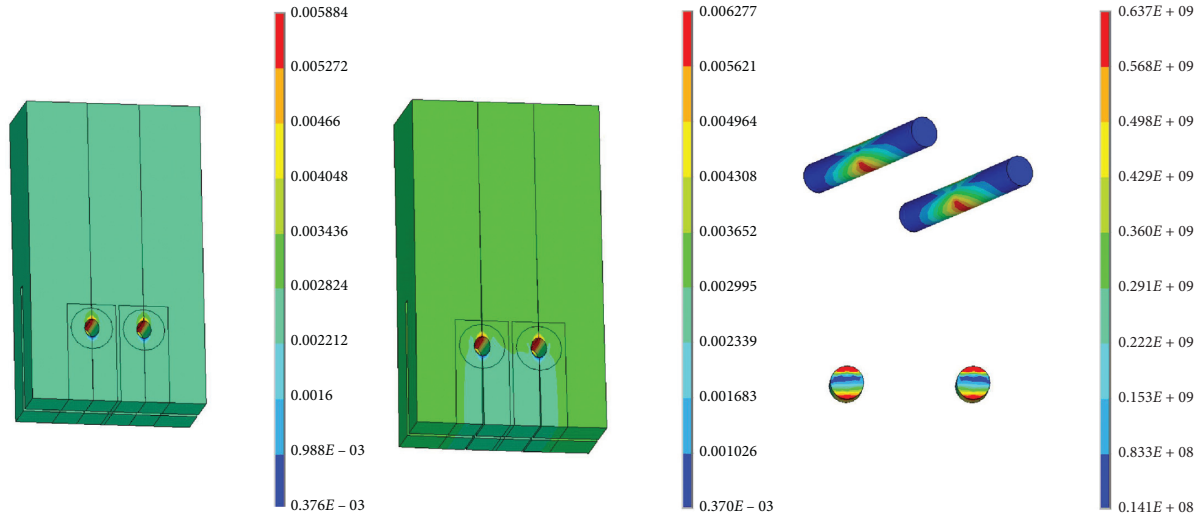

Figure 14: Failure mode of initially perfect Joint 2: (a) embedment deformation of wood; (b) splitting failure in the joint area; (c) von Mises stress distribution of bolts.

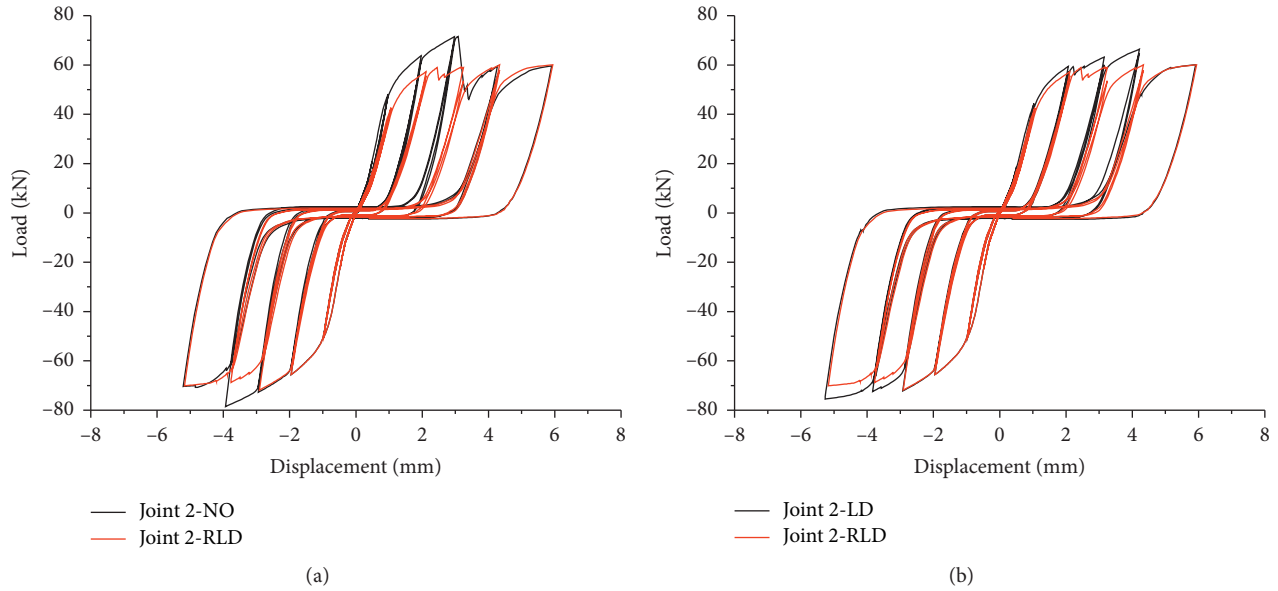

Figure 15: Hysteretic curves of Joint 2: (a) comparison between initially perfect Joint 2 and Joint 2-RDT; (b) comparison between Joint 2-LD and Joint 2-RLD.

$$K_i = \frac{|F_{ip}| + |F_{in}|}{|\Delta_{ip}| + |\Delta_{in}|}, \quad (4)$$

where F_{ip} and Δ_{ip} represent the maximum positive load and corresponding displacement of loading cycle i; F_{in} and Δ_{in} indicate the maximum negative force and corresponding displacement of cycle i. The change of secant stiffness with the increase of displacement is presented in Figure 19. It can be seen that the secant stiffness of the initially perfect joint is the largest in the same loading cycle compared to joints with initial cracks. Also, more numbers of cracks and longer cracks lead to more decrease in the secant stiffness of joints.

At the early loading stage, the gradual growth of secant stiffness is observed with full contact interaction. For initially perfect Joint 1, the largest secant stiffness of 36.5 kN/mm is obtained at the displacement of 0.5 mm, as shown in Figure 19(a). It decreases to 32 kN/mm when the amplitude of the loading cycle rises to 1.0 mm, which is caused by the development of bolt yielding. A deep decrease of secant stiffness is observed with the amplitude level growing to 2 mm due to the occurrence of brittle failure of wood. For Joint 1 with crack pattern DT, the peak secant stiffness is around 26 kN/mm, which is 28.8% lower than the initially perfect joint. A relatively flat segment was observed after the peak point, and a little decrease of secant stiffness occurs

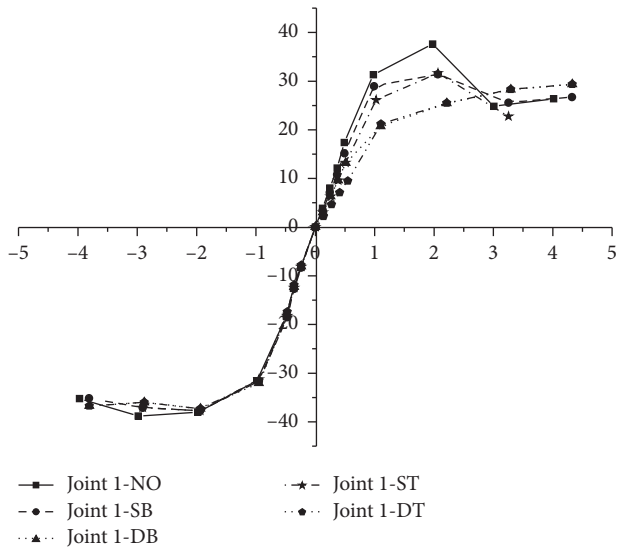

Figure 16: Comparisons of skeleton curves for Joint 1.

Table 3: Summary of the mechanical parameters of Joint 1.

	Joint 1-NO	Joint 1-SB	Joint 1-DB	Joint 1-ST	Joint 1-DT
Elastic stiffness (kN/mm)	32.7/33.6	28.9/33.5	24.5/33.6	24.6/33.5	17.2/33.0
Yield force (kN)	35.8/−36.0	30.5/−35.8	22.4/−35.7	30.3/−35.9	24.1/−35.6
Yield displacement (mm)	1.7/−1.68	1.65/−1.62	1.52/−1.64	1.85/−1.63	1.87/−1.68
Peak load (kN)	37.6/−38.8	31.4/−37.7	29.4/−37.3	31.6/−37.7	29.4/−37.3
Ultimate displacement (mm)	2.55/−3.97	3.27/−3.82	4.33/−3.80	3.02/−3.82	4.33/−3.80
Ductility ratio	1.50/2.36	1.98/2.36	2.85/2.32	1.63/2.34	2.32/2.26

Note. Mechanical parameters are calculated from the positive and negative sides of skeleton curves, respectively.

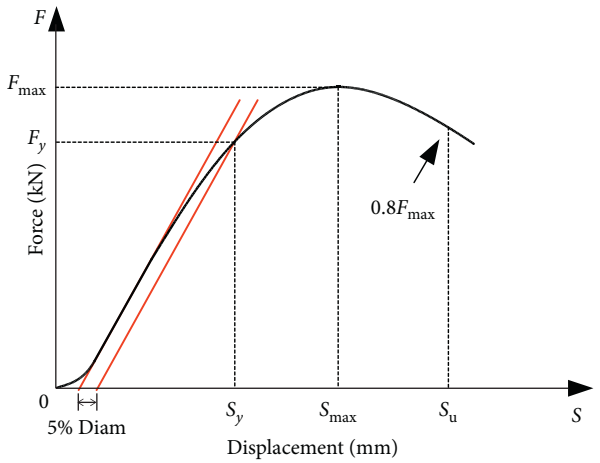

Figure 17: The method of 5% diameter used to determine the yield point.

when the amplitude increases from 0.5 mm to 1.0 mm. It is indicated that the damage accumulation such as bolt yielding and wood locally compression is not significant at the loading stage.

Similar to Joint 1, a first growing tendency of secant stiffness is observed in Joint 2, as shown in Figure 19(b). The largest secant stiffness of the initially perfect joint is 50.9 kN/mm obtained at the displacement of around 1 mm. The peak value of Joint 2-RLD is 45.9 kN/mm, which is decreased by 9.8% with the existence of initial cracks. A rapid drop of secant stiffness is observed after the peak point due to the occurrence of embedment failure of wood. Compared to Figure 19(a), it can be found that the decrease of peak secant stiffness in Joint 2 is much lower than that observed in Joint 1, which indicates that initial cracks have a less dramatic effect on the secant stiffness of bolted joints with embedment failure mode.

4.4. Energy Dissipation. To estimate the accumulative energy dissipation of the joint under reversed cyclic loading, the enclosed area of the hysteretic loop was calculated for each loading cycle based on numerical integration, and the accumulative energy dissipation was presented in Figure 20. As can be seen from Figure 20(a), the energy dissipated in Joint 1 is negligible during the loading cycles with a magnitude lower than 0.5 mm, which indicated that the materials behave elastically at this deformation level. With the displacement increasing from 1.0 mm to 4.0 mm, bolt yielding and obvious bolt bending deformation are observed in the joint, and the energy dissipated grows rapidly. The total energy dissipated in initially perfect Joint 1 is around 677 J. Compared to joints with crack pattern DB and DT, the joints with single crack dissipated more energy at the displacement lower than 4 mm, while similar total energy dissipated of around 514 J is obtained at the end of the loading process.

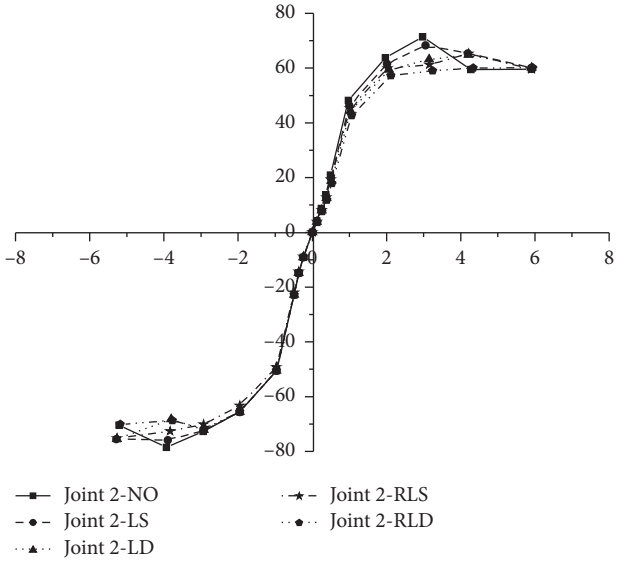

Figure 18: Comparisons of skeleton curves for Joint 2.

Table 4: Summary of the mechanical parameters of Joint 2.

	Joint 2-NO	Joint 2-LS	Joint 2-LD	Joint 2-LRS	Joint 2-LRD
Elastic stiffness (kN/mm)	49.6/52.2	46.2/52.2	42.9/52.2	44.8/50.7	40.2/52.1
Yield force (kN)	61.7/−63.3	60.3/−63.2	57.6/−62.6	59.6/−60.9	56.0/−63.0
Yield displacement (mm)	1.85/−1.79	1.92/−1.79	1.96/−1.81	1.92/−1.79	2.0/−1.82
Peak load (kN)	71.4/−78.6	68.4/−75.8	64.8/−75.5	65.3/−75.1	60.1/−71.8
Ultimate displacement (mm)	5.91/−5.21	5.90/−5.28	5.91/−5.27	5.91/−5.27	5.94/−5.17
Ductility ratio	3.19/2.91	3.08/2.95	3.02/2.91	3.08/2.94	2.94/2.84

Note. Mechanical parameters are calculated from the positive and negative sides of skeleton curves, respectively.

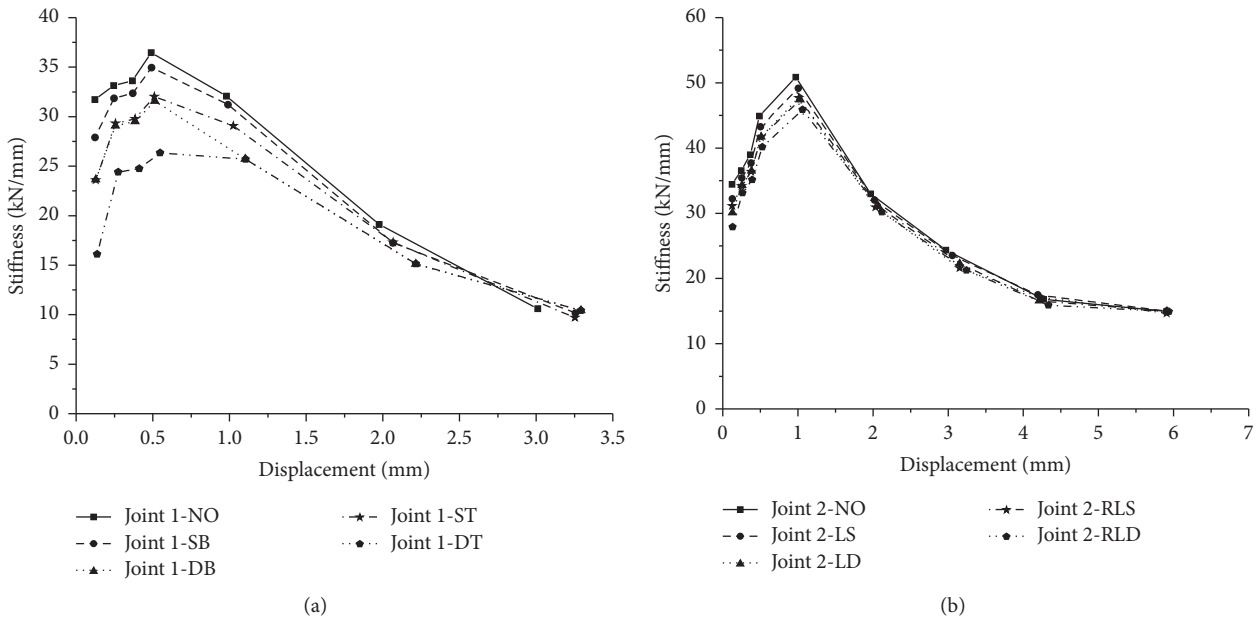

Figure 19: Stiffness degradation observed in bolted glulam joints: (a) Joint 1; (b) Joint 2.

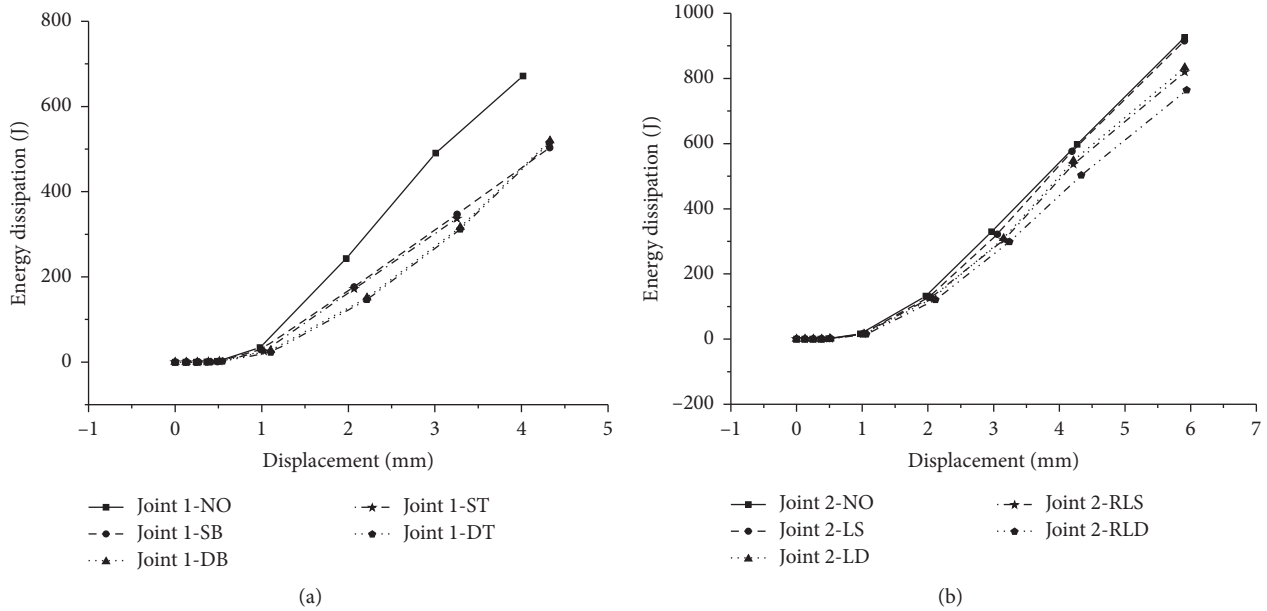

Figure 20: Comparisons of energy dissipation curves: (a) Joint 1; (b) Joint 2.

The energy dissipated of bolted glulam joints with initial cracks is only 76% of the initially perfect joint.

For initially perfect Joint 2, a similar increasing tendency is observed and the total energy dissipated is 932 J. As can be found from Figure 20(b), lower energy dissipated is observed in the joints with more cracks. The total energy dissipated of Joint 2-RLD is 764 J, and the decreasing ratio is 18% compared to the initially perfect joint.

Equivalent viscous damping ratios have been calculated at different amplitude levels as follows:

$$\xi = \frac{1}{2\pi} \cdot \frac{E_p}{E_d}, \tag{5}$$

where E_p represents the enclosed area of the hysteretic loop for each primary loading cycle and E_d equals the area of two triangles ($S_{\Delta OAB} + S_{\Delta OCD}$), as shown in Figure 21. The relationships between equivalent viscous damping ratios and the displacement are presented in Figure 22.

It can be seen from Figure 22(a) that the equivalent viscous damping ratios of Joint 1 are quite low at displacement of 0.5 mm. With the displacement rising from 0.5 mm to 2.0 mm, the damping ratio of the initially perfect joint increases to 0.18 linearly with damage accumulation, and a damping ratio of 0.196 is achieved at the displacement of 3.0 mm. For Joint 1 with initial cracks, the damping ratios increase as the displacement grows from 0.5 mm to 2.0 mm, and a damping ratio of around 0.17 is obtained. The damping ratio is reduced by 13.3% with the existence of initial cracks. After the peak point, a drop of equivalent viscous damping ratio is observed with further application of displacement loading.

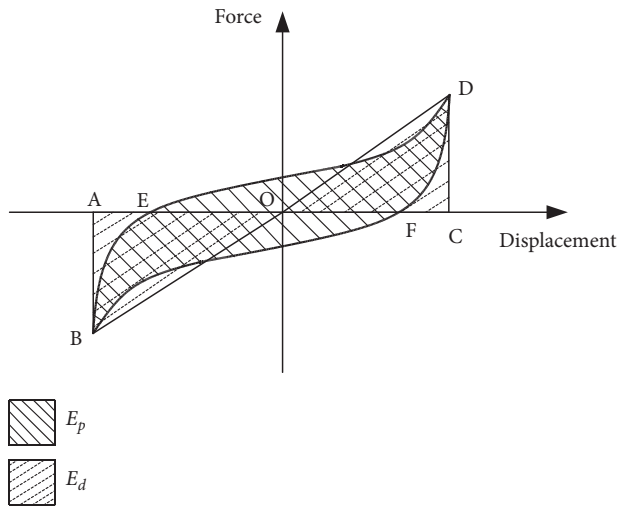

Figure 21: Determination of energy dissipation.

As can be seen from Figure 22(b), a similar changing tendency of equivalent viscous damping ratio is observed in Joint 2 before the displacement reaches 2.0 mm. The equivalent viscous damping ratio of initially perfect Joint 2 is lower than that of Joint 1. A peak damping ratio of 0.114 is obtained at the displacement of 2.0 mm and the damping ratio decreases with further increase in loading amplitude. The damping ratio of Joint 2-LS and Joint 2-RLD is 0.112 and 0.109, respectively. Less significant influence of initial cracks on equivalent viscous damping ratio is observed in Joint 2 when compared to Joint 1.

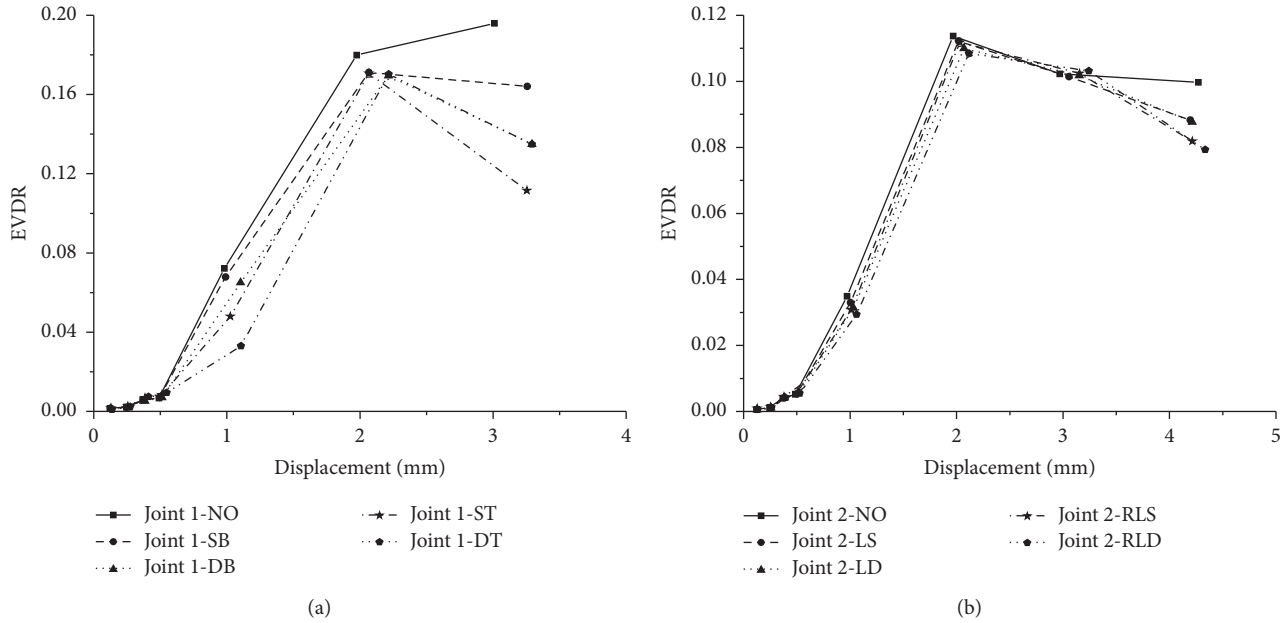

Figure 22: Relationships between equivalent viscous damping ratio and displacement: (a) Joint 1; (b) Joint 2.

5. Conclusion

In the paper, a 3D numerical model was developed to investigate the influence of initial cracks on the cyclic behavior of bolted glulam joints under parallel-to-grain loading. Cohesive zone material law was applied to simulate the propagation of initial cracks and brittle failure of wood. With the application of the Hill yield criterion and wood foundation zone model, the local crushing behavior of wood was reproduced by numerical results. The feasibility of the numerical model was verified by comparison with full-scale experimental results, and different crack patterns and bolt configurations were further considered in a parametric study.

It was found that peak capacity and elastic stiffness of bolted glulam joints were reduced with the existence of initial cracks. More decrease in capacity was observed in joints with more cracks, and longer cracks affect elastic stiffness more dramatically. For Joint 1 with splitting failure occurring under positive loading, the decreasing ratios can be up to 21.8% and 47.4%, respectively. The ductility behavior of Joint 2 with controlled failure mode of wood embedment is impaired by initial cracks. Moreover, under reversed cyclic loading, less energy dissipated is observed in bolted glulam joints with initial cracks, which is only 76% of energy dissipated in the initially perfect joint. Further, the equivalent viscous damping ratio of bolted glulam joint is reduced by 13.3% with the existence of initial cracks.

Data Availability

The data used to support the findings of this study are included within the article and available from the corresponding author upon request.

Conflicts of Interest

The authors declare that they have no conflicts of interest.

Acknowledgments

The authors gratefully acknowledge the National Natural Science Foundation of China (Grant no. 51908147) for supporting this research.

References

[1] R. Y. Itani and K. F. Faherty, *Structural Wood Research: State-of-The-Art and Research Needs*, ASCE, Reston, VA, USA, 1984.

[2] T. V. P. Caldeira, N. Dourado, A. M. P. De Jesus, M. F. S. F. De Moura, and J. J. L. Morais, "Quasi-static behavior of moment-carrying steel-wood doweled joints," *Construction and Building Materials*, vol. 53, pp. 439–447, 2014.

[3] E.-M. Meghlat, M. Oudjene, H. Ait-Aider, and J.-L. Batoz, "A new approach to model nailed and screwed timber joints using the finite element method," *Construction and Building Materials*, vol. 41, pp. 263–269, 2013.

[4] C. L. Santos, A. M. P. De Jesus, J. J. L. Morais, and B. F. C. Fontoura, "An experimental comparison of strengthening solutions for dowel-type wood connections," *Construction and Building Materials*, vol. 46, pp. 114–127, 2013.

[5] P. Zarnani and P. Quenneville, "Strength of timber connections under potential failure modes: an improved design procedure," *Construction and Building Materials*, vol. 60, no. 16, pp. 81–90, 2014.

[6] I. Gavric, M. Fragiacomo, and A. Ceccotti, "Cyclic behaviour of typical metal connectors for cross-laminated (CLT) structures," *Materials and Structures*, vol. 48, no. 6, pp. 1841–1857, 2015.

[7] A. Jorissen and M. Fragiacomo, "General notes on ductility in timber structures," *Engineering Structures*, vol. 33, no. 11, pp. 2987–2997, 2011.

[8] A. Lokaj and K. Klajmonová, "Dowel type joints of round timber exposed to static and cyclic tension forces," *Procedia Engineering*, vol. 114, pp. 240–247, 2015.

[9] M. Popovski, "Seismic performance of braced timber frames," Doctoral dissertation, University of British Columbia, Vancouver, Canada, 2000.

[10] T. L. Wilkinson, "Analysis of nailed joints with dissimilar members," *Journal of the Structural Division*, vol. 98, no. 9, pp. 2005–2013, 1972.

[11] R. O. Foschi and H. Prion, "Behaviour of heavy timber connections under cyclic loads," Thesis, Report, University of British Columbia, Vancouver, B.C., Canada, 1996.

[12] J. Xu and J. D. Dolan, "Development of nailed wood joint element in ABAQUS," *Journal of Structural Engineering*, vol. 135, no. 8, pp. 968–976, 2009.

[13] Y.-L. Shen, J. Schneider, S. Tesfamariam, S. F. Stiemer, and Z.-G. Mu, "Hysteresis behavior of bracket connection in cross-laminated-timber shear walls," *Construction and Building Materials*, vol. 48, pp. 980–991, 2013.

[14] Z. Shu, Z. Li, M. He, X. Zheng, and T. Wu, "Seismic design and performance evaluation of self-centering timber moment resisting frames," *Soil Dynamics and Earthquake Engineering*, vol. 119, pp. 346–357, 2019.

[15] R. O. Foschi, "Load-slip characteristic of nails," *Wood Science*, vol. 7, pp. 69–76, 1974.

[16] J. P. Hong, "Three-dimensional nonlinear finite element model for singe and multiple dowel-type wood connections," Doctoral Dissertation, University of British Columbia, Vancouver, B.C., Canada, 2007.

[17] D. M. Moses and H. G. L. Prion, "Stress and failure analysis of wood composites: a new model," *Composites Part B: Engineering*, vol. 35, no. 3, pp. 251–261, 2004.

[18] N. Kharoufa, G. McClure, and I. Smith, "Elasto-plastic modelling of wood bolted connections," *Computers and Structures*, vol. 81, no. 8-11, pp. 747–754, 2003.

[19] B. H. Xu, A. Bouchaïr, M. Taazount, and E. J. Vega, "Numerical and experimental analyses of multiple-dowel steel-to-timber joints in tension perpendicular to grain," *Engineering Structures*, vol. 31, no. 10, pp. 2357–2367, 2009.

[20] M. Patton-Mallory, P. Pellicane, and F. Smith, "Qualitative assessment of failure in bolted connections: tsai-Wu criterion," *Journal of Testing and Evaluation*, vol. 26, no. 5, pp. 497–505, 1998.

[21] M. Patton-Mallory, P. J. Pellicane, and F. W. Smith, "Modeling bolted connections in wood: review," *Journal of Structural Engineering*, vol. 123, no. 8, pp. 1054–1062, 1997.

[22] N. Dourado, F. G. A. Silva, and M. F. S. F. De Moura, "Fracture behavior of wood-steel dowel joints under quasi-static loading," *Construction and Building Materials*, vol. 176, pp. 14–23, 2018.

[23] J. Zhang, M.-J. He, and Z. Li, "Numerical analysis on tensile performance of bolted glulam joints with initial local cracks," *Journal of Wood Science*, vol. 64, no. 4, pp. 364–376, 2018.

[24] C. L. Santos, A. M. P. De Jesus, J. J. L. Morais, and J. L. P. C. Lousada, "Quasi-static mechanical behaviour of a double-shear single dowel wood connection," *Construction and Building Materials*, vol. 23, no. 1, pp. 171–182, 2009.

[25] J. Sjödin and C.-J. Johansson, "Influence of initial moisture induced stresses in multiple steel-to-timber dowel joints," *Holz als Roh- und Werkstoff*, vol. 65, no. 1, pp. 71–77, 2006.

[26] M. He, J. Zhang, and Z. Li, "Influence of cracks on the mechanical performance of dowel type glulam bolted joints," *Construction and Building Materials*, vol. 153, pp. 445–458, 2017.

[27] J. Zhang, M. He, and Z. Li, "Mechanical performance assessment of bolted glulam joints with local cracks," *Journal of Materials in Civil Engineering*, vol. 30, no. 6, 2018.

[28] E. P. Saliklis, T. J. Urbanik, and B. Tokyay, "Bilinear modelling of cellulosic orthotropic nonlinear materials," *Journal of Pulp and Paper Science*, vol. 29, no. 12, pp. 407–411, 2003.

[29] B. H. Xu, M. Taazount, A. Bouchaïr, and P. Racher, "Numerical 3D finite element modelling and experimental tests for dowel-type timber joints," *Construction and Building Materials*, vol. 23, no. 9, pp. 3043–3052, 2009.

[30] J. L. Jensen and P. Quenneville, "Fracture mechanics analysis of row shear failure in dowelled timber connections," *Wood Science and Technology*, vol. 44, no. 4, pp. 639–653, 2009.

[31] BSI, *Timber Structures-Test Methods-Cyclic Testing of Joints Made with Mechanical Fasteners*, BSI, London, UK, 2001.

[32] BSI, *Mechanical Properties of Fasteners Bolts, Screws and Studs*, BSI, London, UK, 2000.

[33] ASTM, *Standard Test Method for Evaluating Dowel-Bearing Strength of Wood and Woodbase Products*, ASTM, West Conshohocken, PA, USA, 2013.